

Combustion synthesis and characterization of Ni-doped LiMn_2O_4 cathode nanoparticles for lithium ion battery applications

Alagu Segar Deepi¹, Gopalakrishnan Sriresh¹, Arputharaj Samson Nesaraj¹

¹Department of Applied Chemistry, School of Sciences, Arts, Media and Management, Karunya Institute of Technology and Sciences (Deemed to be University), Karunya Nagar, Coimbatore – 641 114, Tamil Nadu, India.
e-mail: dp.vani2412@gmail.com, srireshphd@gmail.com, drsamson@karunya.edu

ABSTRACT

In this research work, fine powders of spinel-type $\text{LiMn}_{2-x}\text{Ni}_x\text{O}_{4-\delta}$ (where $x = 0.1, 0.2, 0.3, 0.4$ and 0.5) as cathode materials for lithium ion batteries were synthesized by combustion synthesis using urea as fuel and metal nitrates as oxidizers at a temperature of 600°C . The physiochemical properties of the prepared cathode materials were investigated by X-ray diffraction (XRD), fourier transform infrared spectroscopy (FTIR), particle size analysis, energy dispersive analysis (EDAX) and scanning electron microscopy (SEM). The electrochemical characteristics were studied by impedance spectroscopy. It was found that the physical characteristics were moderately influenced because of different dopant (Ni) concentration. Among the samples studied, $\text{LiMn}_{1.9}\text{Ni}_{0.1}\text{O}_{4-\delta}$ resulted in better electrical conductivity ($6.49 \times 10^{-5} \text{ Scm}^{-1}$) at room temperature and hence it may be suitable for lithium ion battery applications.

Keywords: Ni doped LiMn_2O_4 , physical characterization, lithium ion battery application

INTRODUCTION

Electrochemical devices, i.e, batteries can convert chemical energy into electrical energy. With increase in the consumption of electronic energy storages in our daily life usage such as portable electronic toys such as laptops, digital cameras, cellular phones and other usages like electric vehicles, hybrid vehicles, military and aerospace which have been developed and explored. The lithium-ion batteries have received much attention as the most viable and eco-friendly power source [1-5]. Furthermore it is an extreme challenging for renewable energy sources like wind and solar energy. The world market has valued billions of dollars for lithium-ion batteries in large scale storage [6-9]. The three dimensional crystal structure of LiMn_2O_4 is one of the most promising cathode materials for its high abundance, low toxicity, high energy density and high excellent voltage characteristics [10-12]. The main usage of Li-ion battery technology reveals that it not only possess high energy density also it is the most electropositive metal [13]. However, LiMn_2O_4 faces some disadvantages by fading in capacity on storage and charge-discharge cycling at certain temperature [14]. Researchers noticed the drawback in loss of capacity of LiMn_2O_4 is because of LiMn_2O_4 include dissolution of a disproportionation of Mn^{3+} into the electrolyte [15], $2\text{Mn}^{3+} \rightarrow \text{Mn}^{2+} + \text{Mn}^{4+}$ at high electrode potential, electrolyte decomposition [16]. In order to improve the performance of LiMn_2O_4 needs a further improvement by doping divalent or trivalent $\text{LiM}_x\text{Mn}_{2-x}\text{O}_4$ spinel phase ($m = \text{Co}, \text{Ni}, \text{Fe}, \text{Cr}$) including by various synthesis such as sol-gel method [17], one-step precipitation method [18], solid-state reaction method [19] and combustion method [20]. Among the above methods, combustion method is a promising technique, which is based on a highly exothermic, self-sustaining reaction generated by heating solution mixture of aqueous metal salts with fuels, such as, urea, glucose, glycine and citric acid. This method has been used efficiently to prepare a variety of oxide materials for the application of energy storage devices such as fuel cells, super capacitors and batteries. It not only yields nanomaterials with very high surface areas but also enables uni-

form (homogenous) doping of trace amounts of various elements in a single step [21-23].

Yu and Zhou have studied the effect of sintering temperature on structure and electrochemical properties of LiMn_2O_4 [24]. It was reported that LiMn_2O_4 suffers from the surface dissolution of manganese in the electrolyte at elevated temperature, especially above 60°C , which leads to a severe capacity fading. To overcome this barrier, LEE *et al.* [25] have developed an imaginative material design; a novel heterostructure. LiMn_2O_4 with epitaxially grown layered ($R\bar{3}m$) surface phase. Mg^{2+} and Ti^{4+} co-doped spinel LiMn_2O_4 lithium-ion cathode material was prepared via a simple high-temperature solid-state route, presenting the high specific capacity, upgraded cyclability, and enhanced rate capability contemporaneously [26]. Among the various dopants reported literature, Ni doping in LiMn_2O_4 is regarded as a typical method to enhance the structural stability and increase in the electrochemical performance of the LiMn_2O_4 material [27]. The importance of doping Ni and also other metals in the LiMn_2O_4 was to weaken the Jahn-Teller effect which results in the improvement of stability of the material and also in the cyclic performance even after 500 cycles [28].

In this research paper, we describe the urea-nitrate based combustion synthesis of Ni doped LiMn_2O_4 fine particles, $\text{LiMn}_{2-x}\text{Ni}_x\text{O}_{4-\delta}$ (where $x = 0.1, 0.2, 0.3, 0.4$ and 0.5) and their physio-chemical / electrochemical characterization for use as cathode material in lithium-ion batteries.

2. MATERIALS AND METHODS

2.1 Materials

Nickel nitrate (98%, Loba Chemie, India), lithium nitrate (98%, Merck, India), manganese nitrate (98%, Merck, India) and urea (99.5%, Merck, India) were used in the preparation of Ni doped / undoped LiMn_2O_4 nanoparticles without further purification. Deionized water was used throughout.

2.2 Methods

2.2.1 Synthesis of $\text{LiMn}_{2-x}\text{Ni}_x\text{O}_{4-\delta}$ nanoparticles

In the typical experiment, stoichiometric amounts of lithium nitrate, manganese nitrate, nickel nitrate were calculated based on propellant chemistry calculations [29] and dissolved in a minimum quantity of distilled water (approximately, 20 ml) along with appropriate quantity of urea as organic fuel. The mixed solution was heated in a mantle at $50 - 70^\circ\text{C}$ and the volume was reduced to half. Afterwards, the solution was introduced into a muffle furnace maintained at 600°C where it boiled, frothed, ignited and caught fire (temperature rise up to $1100 \pm 100^\circ\text{C}$). At these high temperatures, the metal nitrates decomposed to metal oxides of nitrogen and hence acted as oxidizer for further combustion which led to voluminous foamy combustion residue within 5 – 10 minutes. The flame persisted for about 1 minute. The foam was then lightly ground in glass mortar with pestle to obtain fine nanoparticles. The stoichiometric proportion of precursor materials used for the synthesis of Ni doped LiMn_2O_4 oxide nanoparticles is indicated in Table 1.

Table 1: Stoichiometric proportion of the precursor materials used for the synthesis of $\text{LiMn}_{2-x}\text{Ni}_x\text{O}_{4-\delta}$ nanoparticles.

SAMPLES	WEIGHT OF LiNO_3 (g)	WEIGHT OF $\text{Mn}(\text{NO}_3)_2 \cdot 4\text{H}_2\text{O}(\text{g})$	WEIGHT OF $\text{Ni}(\text{NO}_3)_2 \cdot 6\text{H}_2\text{O}(\text{g})$	WEIGHT OF Urea (g)
LiMn_2O_4	0.689	--	5.02	2.498
$\text{LiMn}_{1.9}\text{Ni}_{0.1}\text{O}_{4-\delta}$	0.689	0.290	4.769	2.503
$\text{LiMn}_{1.8}\text{Ni}_{0.2}\text{O}_{4-\delta}$	0.689	0.581	4.518	2.506
$\text{LiMn}_{1.7}\text{Ni}_{0.3}\text{O}_{4-\delta}$	0.689	0.872	4.267	2.506
$\text{LiMn}_{1.6}\text{Ni}_{0.4}\text{O}_{4-\delta}$	0.689	1.163	4.016	2.505
$\text{LiMn}_{1.5}\text{Ni}_{0.5}\text{O}_{4-\delta}$	0.689	1.453	3.765	2.505

The stoichiometric redox reactions between nitrate salt precursors and urea fuel to produce $\text{LiMn}_{2-x}\text{Ni}_x\text{O}_{4-\delta}$ (where $x = 0, 0.1, 0.2, 0.3, 0.4$ and 0.5) nanoparticles can be represented by a common theoretical equation - 1.



The mechanism for the above reaction is reported as follows in the literature [30]. The metal nitrate – fuel mixture reaction involve dehydration, decomposition, swelling and burn. When urea ($\text{CO}(\text{NH}_2)_2$) is used as a fuel, the probable mechanism involves melting and dehydration in the first few minutes, then the mixture decomposes, with frothing that may be due to the formation of metal-(OH)(NO_3)₂ gel along with other products urea nitrate ($\text{CH}_5\text{N}_3\text{O}_4$), ($\text{H}_2\text{N-CO-NH-CO-NH}_2$) (biuret), HNCO, and NH_3 . It then foams, due to the gaseous decomposition products of the intermediates, causing enormous swelling of the reaction product. The gaseous decomposition product is a mixture of N_2 , NH_3 and HNCO, which are combustible. Finally, the accumulation of the combustible mixture of gases causes the foam to burst into flame and burn into incandescence, with further swelling, producing a doped oxide powder.

2.3 Physical characterization

The powder XRD study was carried out using a Shimadzu XRD6000 X-ray diffractometer at a scan speed of 5 deg/min using $\text{CuK}\alpha$ radiation. The crystallite sizes of the ceramic powders were calculated by Scherrer's formula. FTIR spectra of all the samples were studied by Shimadzu IR Prestige – 21 model FTIR spectrometer. The particle size of the powder was measured using Malvern particle size analyzer (Malvern Instruments, Worcestershire, UK) using triple distilled water as medium. The morphology of the particles and percentage of elements present in the samples (EDAX) was studied by means of JEOL Model JSM-6360 scanning electron microscope (JEOL Ltd., Tokyo, Japan).

2.4 Electrochemical characterization

The resultant Ni doped LiMn_2O_4 materials was ground into a fine powder with addition of PVA binder solution, mixed well, dried and placed in a die. A pressure of around 4000 kg/cm^2 was been applied to form the pellet with a thickness in the range of 1.4-1.5 cm and a diameter of 1 cm. After this process, the pellets were sintered at 600°C for 6 hrs before subjecting them for conductivity studies. The electrochemical impedance studies were conducted using an electrochemical work station with two electrode system under aluminium foil substrate in the frequency range of 40 Hz – 1 MHz at room temperature.

3. RESULTS AND DISCUSSIONS

3.1 XRD Studies

Figure 1 shows the XRD pattern obtained on the pure LiMn_2O_4 and Ni doped LiMn_2O_4 nanoparticles prepared by combustion technique using urea as organic fuel.

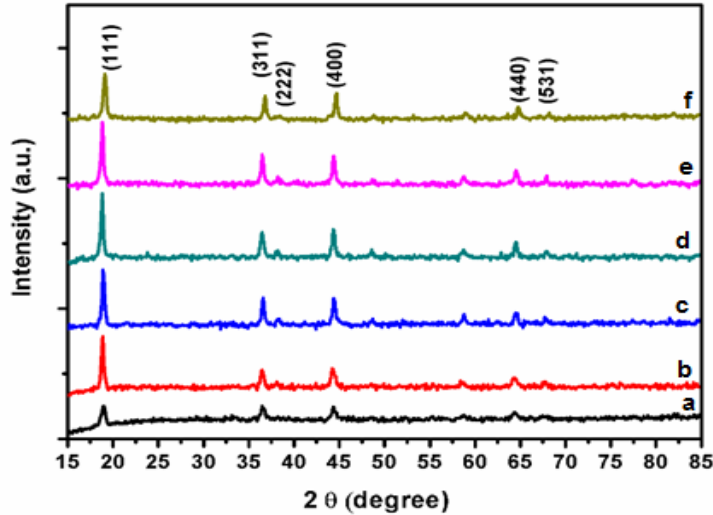


Figure 1: XRD patterns obtained on parent LiMn_2O_4 and Ni doped LiMn_2O_4 such as a) pure LiMn_2O_4 ; b) $\text{LiMn}_{1.9}\text{Ni}_{0.1}\text{O}_{4-\delta}$; c) $\text{LiMn}_{1.8}\text{Ni}_{0.2}\text{O}_{4-\delta}$; d) $\text{LiMn}_{1.7}\text{Ni}_{0.3}\text{O}_{4-\delta}$; e) $\text{LiMn}_{1.6}\text{Ni}_{0.4}\text{O}_{4-\delta}$; f) $\text{LiMn}_{1.5}\text{Ni}_{0.5}\text{O}_{4-\delta}$ nanoparticles prepared by combustion technique.

The existence of well-defined and highly intense Bragg peaks demonstrated that the synthesized products are phase pure and highly crystalline in nature. The obtained diffraction peaks of both LiMn_2O_4 and Ni doped LiMn_2O_4 are well in agreement with standard diffraction data (JCPDS no: 89-8325) for LiMn_2O_4 and confirmed the existence of spinel cubic type crystalline structure with $Fd\bar{3}m$ space group in the samples. No other secondary or impurity peaks observed in the samples. The crystallite sizes have been calculated by Scherrer's equation (2).

$$D = \frac{K \lambda}{\beta \cos \theta} \quad (2)$$

where 'D' is the crystallite size, 'k' is the numerical constant (~ 0.9), ' λ ' is the wavelength of x-rays (for $\text{CuK}\alpha$ radiation, $\lambda = 1.5418 \text{ \AA}$), ' β ' is the effective broadening taken as a full width at half maximum (FWHM) (in radians), ' θ ' is the diffraction angle for the peak. The calculated average crystallite size is found to be 10.6 to 24.7 nm respectively. Crystallography parameters obtained on Ni doped LiMn_2O_4 nanoparticles are given in Table.2. The XRD data of $\text{LiMn}_{2-x}\text{Ni}_x\text{O}_{4-\delta}$ is in line with the reported data [31]. From this, we could understand that when high concentration of dopants is added the intensity of peaks gets increased, however, pure LiMn_2O_4 resulted with low intensity peaks. Therefore, the crystalline behavior of the materials is highly dependent on dopant concentration. LiMn_2O_4 with high dopant concentration will have high crystalline characteristics than others.

Table 2: Crystallographic parameters obtained on $\text{LiMn}_{2-x}\text{Ni}_x\text{O}_{4-\delta}$ nanoparticles.

SAMPLES	CRYSTAL STRUCTURE	UNIT CELL PARAMETER 'a' (\AA)	UNIT CELL VOLUME (\AA^3)	CRYSTALLITE SIZE (nm)
LiMn_2O_4	Cubic spinel	8.119	535.18	10.6
$\text{LiMn}_{1.9}\text{Ni}_{0.1}\text{O}_{4-\delta}$	Cubic spinel	8.149	541.14	23
$\text{LiMn}_{1.8}\text{Ni}_{0.2}\text{O}_{4-\delta}$	Cubic spinel	8.117	534.79	23.6

$\text{LiMn}_{1.7}\text{Ni}_{0.3}\text{O}_{4-\delta}$	Cubic spinel	8.169	545.13	24.2
$\text{LiMn}_{1.6}\text{Ni}_{0.4}\text{O}_{4-\delta}$	Cubic spinel	8.163	543.93	24.7
$\text{LiMn}_{1.5}\text{Ni}_{0.5}\text{O}_{4-\delta}$	Cubic spinel	8.047	521.07	21.2

3.2 FTIR Studies

Figure 2 shows the FTIR spectra obtained on the pure LiMn_2O_4 and Ni doped LiMn_2O_4 nanoparticles prepared by combustion technique using urea as organic fuel in the range of 4000 to 400 cm^{-1} . The broader peak appeared at 498.58 cm^{-1} in the prepared samples can be ascribed to the metal oxygen vibrations, i.e., Li-O / Ni-O and the peaks appeared between 615 to 624 cm^{-1} can be due to Li-Mn-O. The peaks found near 1506.47 cm^{-1} are due to Li-O bending vibration modes in the samples. The intensity of the IR spectra increases while increasing Ni dopant level. This means that the stability of the LiMn_2O_4 structure is enhanced and which may result in better electrochemical performance. Appearance of broad band near 2900 cm^{-1} corresponds to O-H stretching frequency of the water or moisture [32, 33].

3.3 Particle size measurements

The particle size patterns of the Ni doped LiMn_2O_4 nanoparticles prepared by combustion technique are shown in Figure 3. For all the measurements, 0.01g of sample was sonicated in 30 ml triple distilled water for about 10 minutes and after that the sample was subjected for particle size analysis. The particle size distribution data is indicated in Table.3. The particle are present in the range of $234 - 329\text{ nm}$. The presence of bigger particles ($> 200\text{ nm}$) in the sample may be due to high temperature treatment.

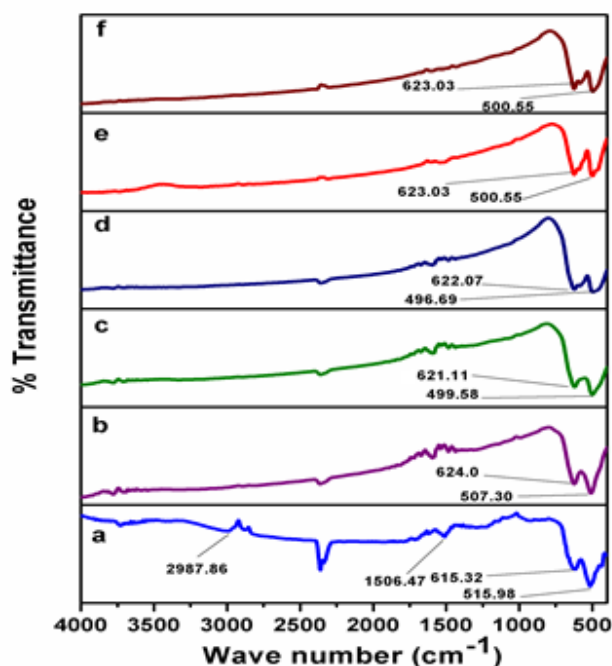


Figure 2: FTIR spectra obtained on parent LiMn_2O_4 and Ni doped LiMn_2O_4 such as a) pure LiMn_2O_4 ; b) $\text{LiMn}_{1.9}\text{Ni}_{0.1}\text{O}_{4-\delta}$; c) $\text{LiMn}_{1.8}\text{Ni}_{0.2}\text{O}_{4-\delta}$; d) $\text{LiMn}_{1.7}\text{Ni}_{0.3}\text{O}_{4-\delta}$; e) $\text{LiMn}_{1.6}\text{Ni}_{0.4}\text{O}_{4-\delta}$; f) $\text{LiMn}_{1.5}\text{Ni}_{0.5}\text{O}_{4-\delta}$ nanoparticles prepared by combustion technique.

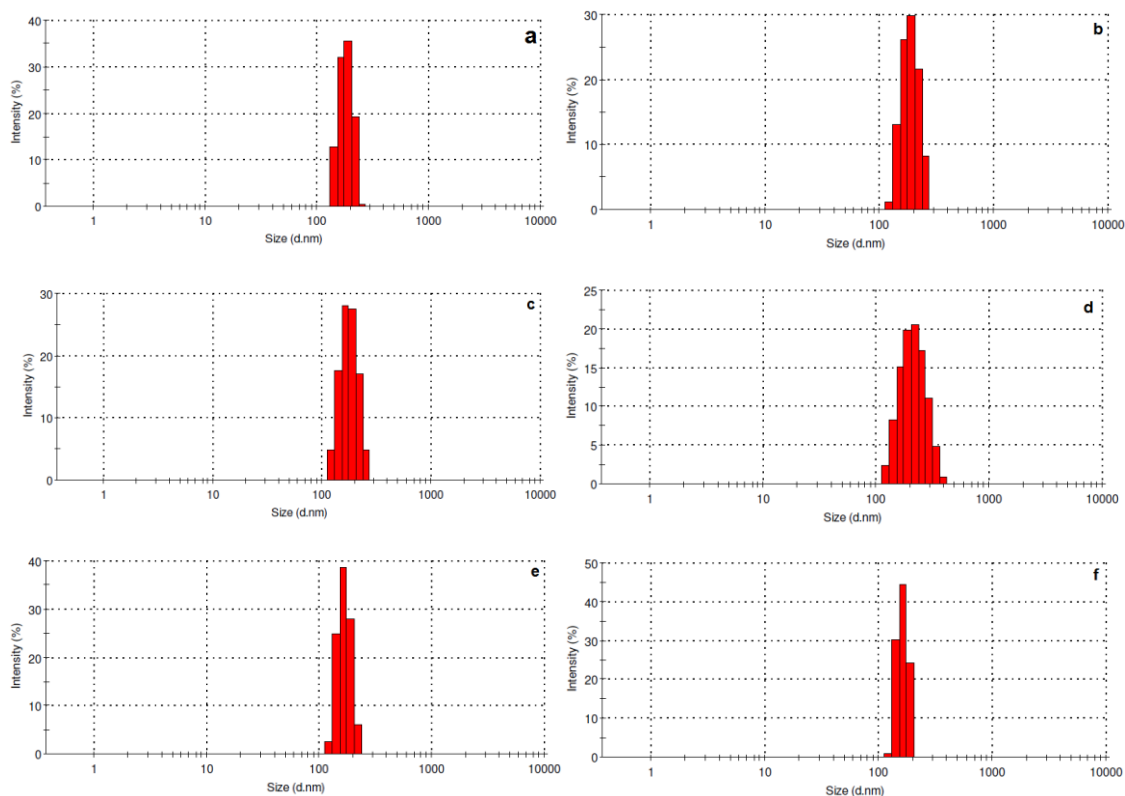


Figure 3: Particle size patterns obtained on parent LiMn_2O_4 and Ni doped LiMn_2O_4 such as a) pure LiMn_2O_4 ; b) $\text{LiMn}_{1.9}\text{Ni}_{0.1}\text{O}_{4-\delta}$; c) $\text{LiMn}_{1.8}\text{Ni}_{0.2}\text{O}_{4-\delta}$; d) $\text{LiMn}_{1.7}\text{Ni}_{0.3}\text{O}_{4-\delta}$; e) $\text{LiMn}_{1.6}\text{Ni}_{0.4}\text{O}_{4-\delta}$; f) $\text{LiMn}_{1.5}\text{Ni}_{0.5}\text{O}_{4-\delta}$ nanoparticles prepared by combustion technique.

Table 3: Particle characteristics data obtained on $\text{LiMn}_{2-x}\text{Ni}_x\text{O}_{4-\delta}$ nanoparticles.

SAMPLES	PEAK 1		AVERAGE PARTICLE SIZE (nm)
	% INTENSITY	DIAMETER (nm)	
LiMn_2O_4	100	181.7	294.9
$\text{LiMn}_{1.9}\text{Ni}_{0.1}\text{O}_{4-\delta}$	100	188.1	242.9
$\text{LiMn}_{1.8}\text{Ni}_{0.2}\text{O}_{4-\delta}$	100	179.4	234.9
$\text{LiMn}_{1.7}\text{Ni}_{0.3}\text{O}_{4-\delta}$	100	218.7	236.7
$\text{LiMn}_{1.6}\text{Ni}_{0.4}\text{O}_{4-\delta}$	100	168.2	327.6
$\text{LiMn}_{1.5}\text{Ni}_{0.5}\text{O}_{4-\delta}$	100	163.4	329.9

3.4 SEM studies

The SEM photographs of the Ni doped LiMn_2O_4 nanoparticles prepared by combustion technique are displayed in Figure 4. From the SEM photographs, it was noticed that compared to the parent LiMn_2O_4 compound, Ni doped LiMn_2O_4 nanomaterials are homogenous along with the presence of few larger particles. The presence of bigger particles in the samples such as $\text{LiMn}_{1.9}\text{Ni}_{0.1}\text{O}_{4-\delta}$, $\text{LiMn}_{1.8}\text{Ni}_{0.2}\text{O}_{4-\delta}$, $\text{LiMn}_{1.7}\text{Ni}_{0.3}\text{O}_{4-\delta}$, $\text{LiMn}_{1.6}\text{Ni}_{0.4}\text{O}_{4-\delta}$ and $\text{LiMn}_{1.5}\text{Ni}_{0.5}\text{O}_{4-\delta}$ may due to the agglomeration of few nanoparticles together at high temperature.

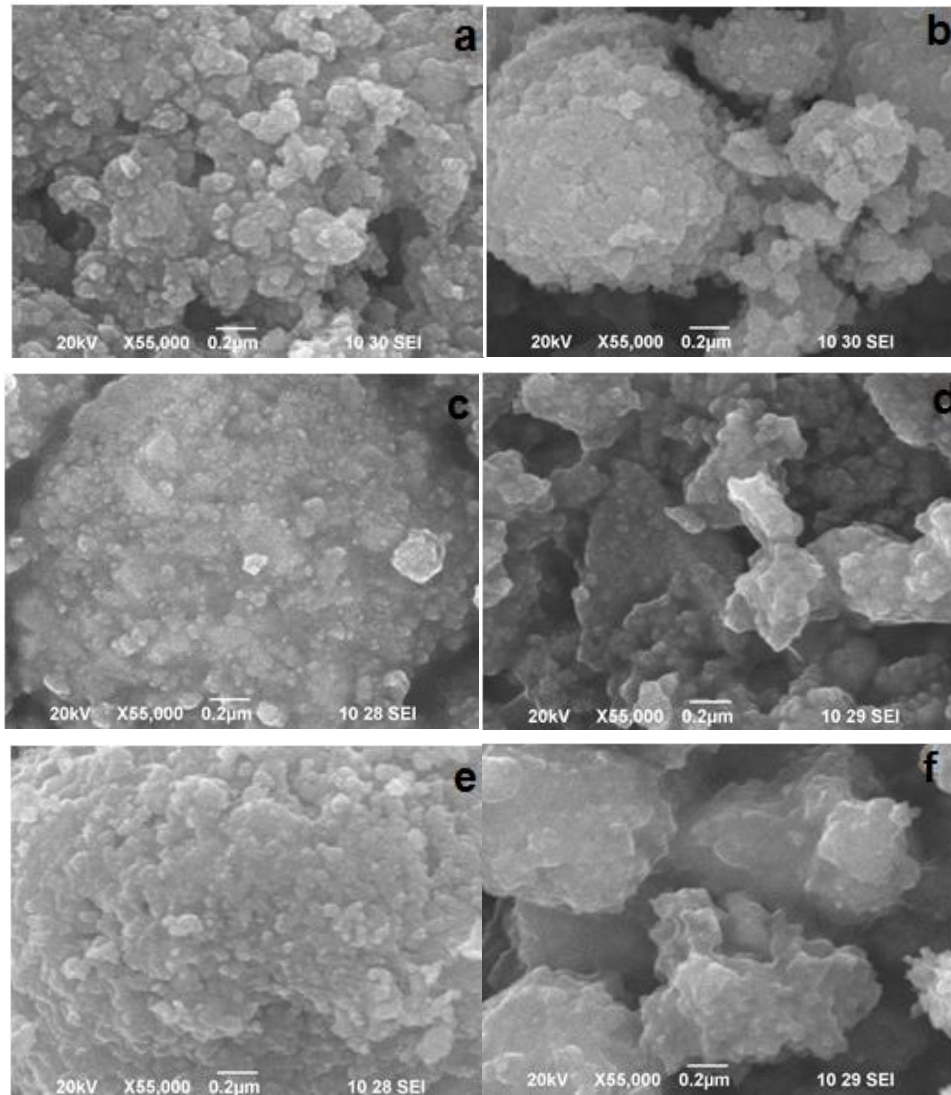
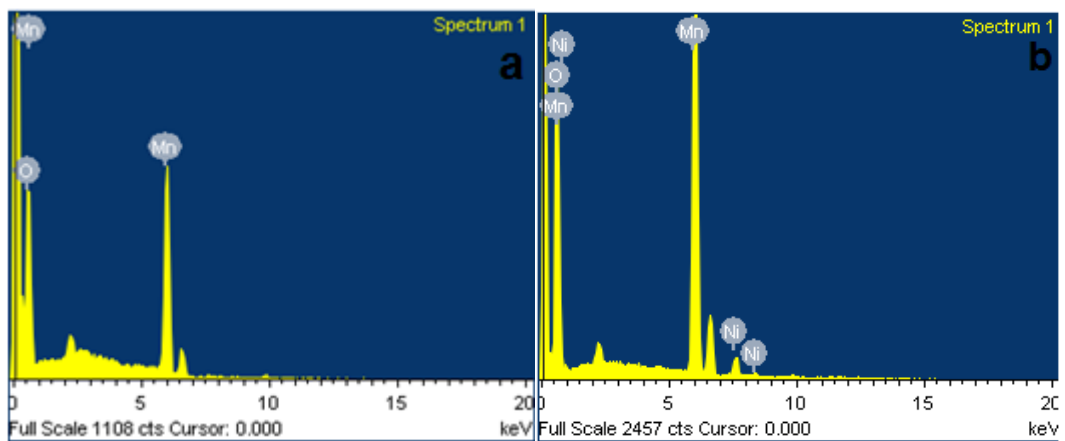


Figure 4: SEM photographs obtained on parent LiMn_2O_4 and Ni doped LiMn_2O_4 such as a) pure LiMn_2O_4 ; b) $\text{LiMn}_{1.9}\text{Ni}_{0.1}\text{O}_{4-\delta}$; c) $\text{LiMn}_{1.8}\text{Ni}_{0.2}\text{O}_{4-\delta}$; d) $\text{LiMn}_{1.7}\text{Ni}_{0.3}\text{O}_{4-\delta}$; e) $\text{LiMn}_{1.6}\text{Ni}_{0.4}\text{O}_{4-\delta}$; f) $\text{LiMn}_{1.5}\text{Ni}_{0.5}\text{O}_{4-\delta}$ nanoparticles prepared by combustion technique.



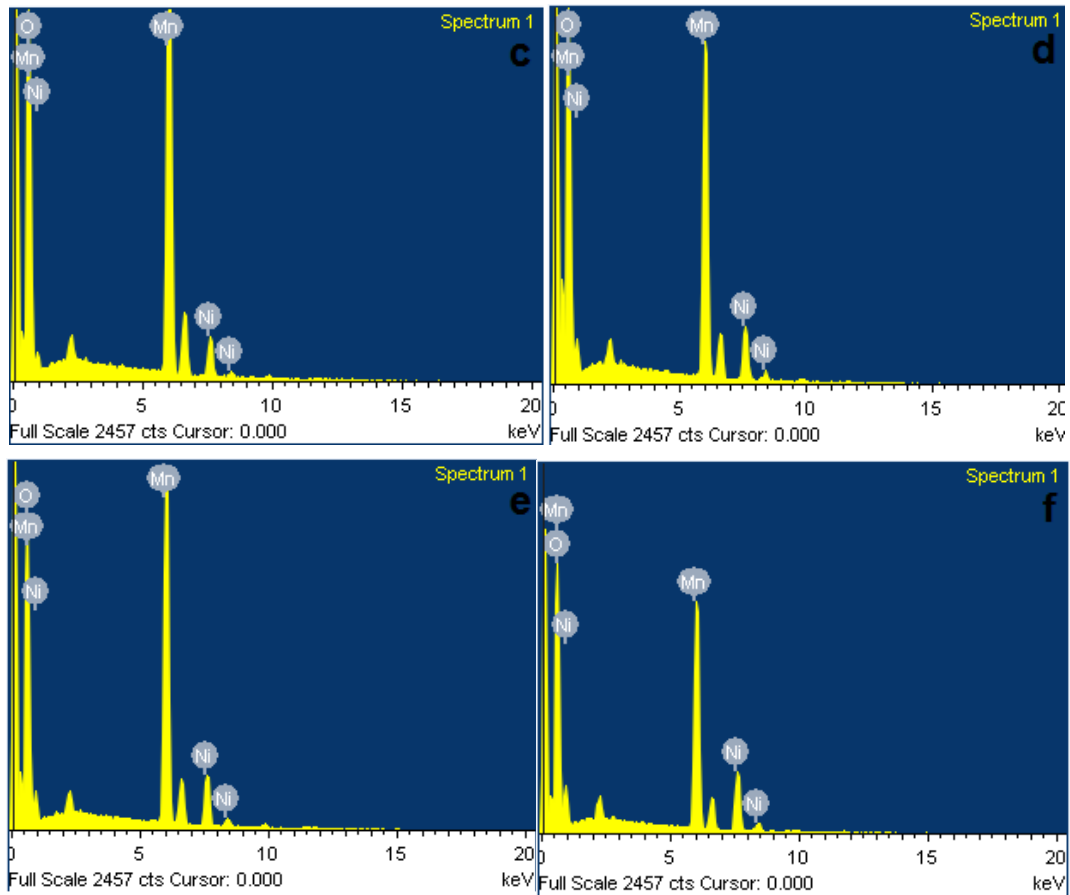


Figure 5:EDAX obtained on nanocrystalline materials such as a) pure LiMn_2O_4 ; b) $\text{LiMn}_{1.9}\text{Ni}_{0.1}\text{O}_{4-\delta}$; c) $\text{LiMn}_{1.8}\text{Ni}_{0.2}\text{O}_{4-\delta}$; d) $\text{LiMn}_{1.7}\text{Ni}_{0.3}\text{O}_{4-\delta}$; e) $\text{LiMn}_{1.6}\text{Ni}_{0.4}\text{O}_{4-\delta}$; f) $\text{LiMn}_{1.5}\text{Ni}_{0.5}\text{O}_{4-\delta}$ nanoparticles prepared by combustion technique.

3.5 Electrochemical impedance studies

Figure 6 displays the typical Nyquist ac impedance plots obtained on the Ni doped LiMn_2O_4 cathode materials in the frequency range of 40 Hz to 1 MHz in the amplitude of 0.05 V at room temperature in the two electrode system. The electrochemical impedance measurements were carried out for all the sintered pellets. The pellets were kept in between the conducting aluminium foils like a sandwich and the measurements were made in air. From the impedance data conductivity values were calculated by using Equation.

$$\sigma = d/R_b S \quad (3)$$

σ = ionic conductivity

Table 4: Chemical composition data obtained on $\text{LiMn}_{2-x}\text{Ni}_x\text{O}_{4-\delta}$ nanoparticles by EDAX analysis.

SAMPLES	ATOMIC % OF ELEMENTS		
	Mn	Ni	O
LiMn_2O_4	31.61	--	68.39
$\text{LiMn}_{1.9}\text{Ni}_{0.1}\text{O}_{4-\delta}$	27.94	1.32	70.74
$\text{LiMn}_{1.8}\text{Ni}_{0.2}\text{O}_{4-\delta}$	24.29	2.76	72.75
$\text{LiMn}_{1.7}\text{Ni}_{0.3}\text{O}_{4-\delta}$	18.42	3.55	78.02
$\text{LiMn}_{1.6}\text{Ni}_{0.4}\text{O}_{4-\delta}$	22.14	3.94	73.92

$\text{LiMn}_{1.5}\text{Ni}_{0.5}\text{O}_{4.6}$	17.36	5.75	76.89
--	-------	------	-------

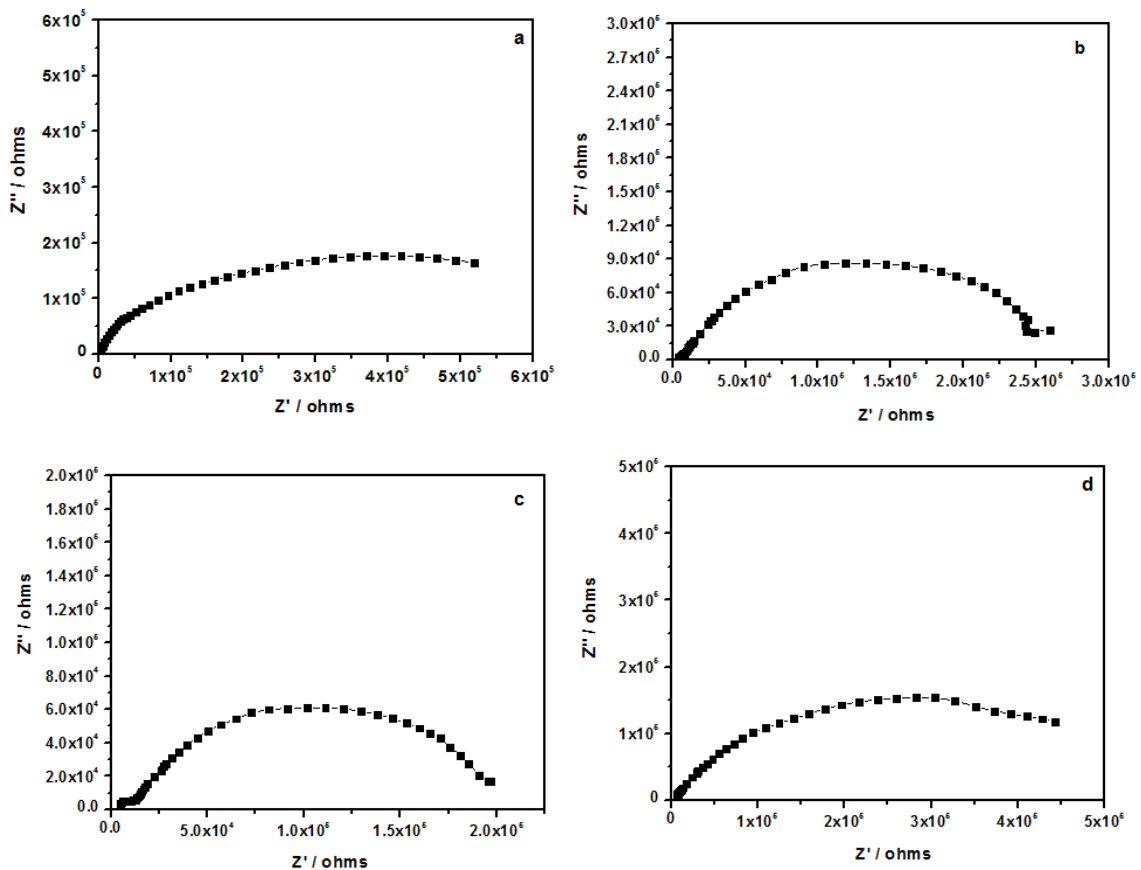
d = thickness of the sample

S = area of the sample

R_b = bulk resistance

Fitting of the measurement data was performed with the software Zview software. The impedance data of the LiMn_2O_4 and Ni doped LiMn_2O_4 oxide pellets fitted with an equivalent circuit as indicated in Figure 7.

The impedance spectra was fitted to the conventional equivalent electronic circuit containing three Resistance-Constant Phase Element (R-CPE) sub circuits in series, which generates two semicircles on the Nyquist plots at the room temperature. The electrical conduction of Ni doped LiMn_2O_4 based materials results from impurity and intrinsic factors. At room temperatures, its conduction is dominated by the dissociated electron concentration from the energy gap of the impurity, whose activation energy of electrical conduction is much lower than that of the intrinsic conduction [34-36]. The conductivity decreases is predominantly due to the addition of nickel. The electrons from the energy gap of the impurity are all dissociated and activated.



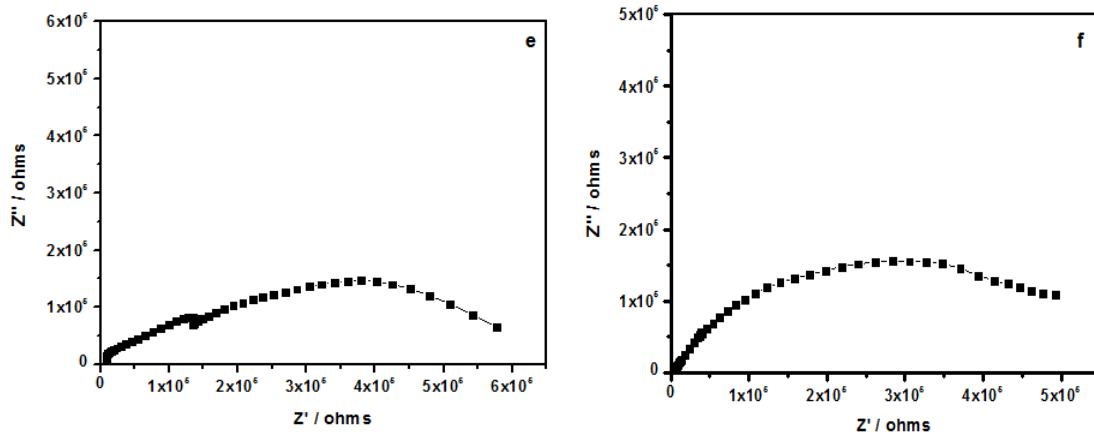


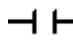
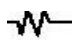
Figure 6: Electrochemical impedance spectra obtained on sintered cathode specimens a) pure LiMn_2O_4 ; b) $\text{LiMn}_{1.9}\text{Ni}_{0.1}\text{O}_{4-\delta}$; c) $\text{LiMn}_{1.8}\text{Ni}_{0.2}\text{O}_{4-\delta}$; d) $\text{LiMn}_{1.7}\text{Ni}_{0.3}\text{O}_{4-\delta}$; e) $\text{LiMn}_{1.6}\text{Ni}_{0.4}\text{O}_{4-\delta}$; f) $\text{LiMn}_{1.5}\text{Ni}_{0.5}\text{O}_{4-\delta}$ at room temperature.

Table 5: Conductivity values calculated for sintered LiMn_2O_4 and Ni doped LiMn_2O_4 compacts using electrochemical impedance spectroscopy at room temperature.

SAMPLES	ELECTRICAL CONDUCTIVITY (Scm^{-1})
LiMn_2O_4	1.58×10^{-6}
$\text{LiMn}_{1.9}\text{Ni}_{0.1}\text{O}_{4-\delta}$	6.49×10^{-5}
$\text{LiMn}_{1.8}\text{Ni}_{0.2}\text{O}_{4-\delta}$	1.6×10^{-6}
$\text{LiMn}_{1.7}\text{Ni}_{0.3}\text{O}_{4-\delta}$	1.95×10^{-6}
$\text{LiMn}_{1.6}\text{Ni}_{0.4}\text{O}_{4-\delta}$	1.32×10^{-6}
$\text{LiMn}_{1.5}\text{Ni}_{0.5}\text{O}_{4-\delta}$	1.67×10^{-6}



Figure 7: Equivalent circuit, used to fit measurement data obtained LiMn_2O_4 and Ni doped LiMn_2O_4 oxide pellets.

(Where, the symbol  referred as capacitor (constant phase element, CPE) and the symbol  referred as resistor)

The bulk conductivity was calculated from the impedance plot and reported in the Table 5. Among the samples studied, $\text{LiMn}_{1.9}\text{Ni}_{0.1}\text{O}_{4-\delta}$ shown better conductivity ($6.49 \times 10^{-5} \text{ S/cm}$). However, all other samples have shown moderate conductivity values which may be useful for Li-ion battery application.

4. CONCLUSIONS

In the present work, a set of LiMn_2O_4 and Ni doped LiMn_2O_4 such as $\text{LiMn}_{1.9}\text{Ni}_{0.1}\text{O}_{4-\delta}$, $\text{LiMn}_{1.8}\text{Ni}_{0.2}\text{O}_{4-\delta}$, $\text{LiMn}_{1.7}\text{Ni}_{0.3}\text{O}_{4-\delta}$, $\text{LiMn}_{1.6}\text{Ni}_{0.4}\text{O}_{4-\delta}$ and $\text{LiMn}_{1.5}\text{Ni}_{0.5}\text{O}_{4-\delta}$ based cathode materials were prepared by combustion route using urea as an organic fuel. The physico-chemical studies, such as, effect of Ni doping on the phase structure of LiMn_2O_4 , structural, particle and morphological performances were studied for all the prepared materials and results found good in comparison with the reported data. The electrochemical characteristics

for Ni doped LiMn_2O_4 by impedance spectroscopy were also measured. Among the samples studied, $\text{LiMn}_{1.9}\text{Ni}_{0.1}\text{O}_{4-\delta}$ cathode has resulted in better conductivity of $6.49 \times 10^{-5} \text{ Scm}^{-1}$. Hence, it may be suitable as cathode for Li-ion battery applications.

5. ACKNOWLEDGEMENTS

The authors AD and ASN thank Karunya Institute of Technology and Sciences for promoting nano-electrochemistry research activity in the Department of Applied Chemistry. One of the authors (G.S.) thanks University Grants Commission, India (UGC, Government of India) for providing Rajiv Gandhi Fellowship for Students with Disability (No. F./2013-14/RGNF-2013-14D-O BC-TAM-56465).

6. BIBLIOGRAPHY

- [1] LIU, D., TROTTIER, J., CHAREST, P., *et al.*, Effect of nano LiFePO_4 coating on $\text{LiMn}_{1.5}\text{Ni}_{0.5}\text{O}_4$ 5 V cathode for lithium ion batteries, *Journal of Power Sources*, v. 204, pp. 127-132, April 2012.
- [2] YANG, S., CHEN, J., LIU, Y., *et al.*, Preparing $\text{LiNi}_{0.5}\text{Mn}_{1.5}\text{O}_4$ nanoplates with superior properties in lithium-ion batteries using bimetal-organic coordination-polymers as precursors, *Journal of Materials Chemistry A*, v. 2, pp. 9322 – 9330, June 2014.
- [3] SUN, X., HAO, G.P., LU, X., *et al.*, High-defect hydrophilic carbon cuboids anchored with Co/CoO nanoparticles as highly efficient and ultra-stable lithium-ion battery anodes, *Journal of Materials Chemistry A*, v. 4, pp. 10166 -10173, July 2016.
- [4] SUN, X., YAN, C., Y. CHEN, *et al.*, Three-dimensionally “curved” NiO nanomembranes as ultrahigh rate capability anodes for Li-ion batteries with long cycle lifetimes, *Advanced Energy Materials*, v. 4, n. 4, pp.1300912, October 2013.
- [5] SUN, X., SI, W., XI, L., *et al.*, In situ-formed, amorphous, oxygen-enabled germanium anode with robust cycle life for reversible lithium storage, *ChemElectroChem*, v. 2, n. 5, pp. 737 – 742, February 2015.
- [6] DENG, Y., MOU, J., WU, H., *et al.*, Enhanced Electrochemical Performance in Ni-Doped LiMn_2O_4 - Based Composite Cathodes for Lithium-Ion Batteries. *ChemElectroChem*, v. 4, n. 6, pp. 1362–1371, March 2017.
- [7] PRIYONO, S., GINTING, N.R., HUMAIDI, S., *et al.*, Synthesis of lithium manganese dioxide (LiMn_2O_4) for lithium-ion battery cathode from various lithium sources, *J. Physics: Conference Series*, v. 985, pp. 012054, 2018.
- [8] LIPU, M.S.H., HANNAN, M.A., HUSSAIN, A., *et al.*, A review of state of health and remaining useful life estimation methods for lithium-ion battery in electric vehicles: challenges and recommendations. *Journal of Cleaner Production*, v. 205, pp.115–133, 2018.
- [9] LIU, D., FAN, X., LI, Z., *et al.*, A cation/ anion co-doped $\text{Li}_{1.12}\text{Na}_{0.08}\text{Ni}_{0.2}\text{Mn}_{0.6}\text{O}_{1.95}\text{F}_{0.05}$ cathode for lithium ion batteries, *Nano Energy*, v.58, pp. 786-796, 2019.
- [10] YAMADA, A., MIURA, K., HINOKUMA K, *et al.*, Synthesis and structural aspects of $\text{LiMn}_2\text{O}_{4\pm\delta}$ as a cathode for rechargeable lithium batteries, *Journal of The Electrochemical Society*, v. 142, n. 7, pp. 2149 – 2156, 1995.
- [11] PARK, H.S., HWANG, S.J., CHOY, J.H., Relationship between chemical bonding character and electrochemical performance in nickel-substituted lithium manganese oxides, *The Journal of Physical Chemistry B*, v. 105, n. 21, pp. 4860-4866, May 2001.
- [12] KOVACHEVA, D., GADJOV, H., PETROV, K., *et al.*, Synthesizing nanocrystalline LiMn_2O_4 by a combustion route, *Journal of Materials Chemistry*, v. 12, n. 4, pp. 1184-1188, March 2002.
- [13] YU, Y., XIANG, M., GUO, J., *et al.*, Enhancing high-rate and elevated-temperature properties of Ni-Mg co-doped LiMn_2O_4 cathodes for Li-ion batteries, *Journal of Colloid and Interface Science*, v. 555, pp. 64–71, 2019.
- [14] SUN, Y.-K., YOON, C.S., KIM, C.K., *et al.*, Degradation mechanism of spinel $\text{LiAl}_{0.2}\text{Mn}_{1.8}\text{O}_4$ cathode materials on high temperature cycling, *Journal of Materials Chemistry*, v. 11, n. 10, pp. 2519 – 2522,

August 2001.

- [15] TARASCON, J.M., MCKINNON, W.R., COOWAR, F., *et al.*, Synthesis Conditions and Oxygen Stoichiometry Effects on Li Insertion into the Spinel LiMn_2O_4 , *Journal of The Electrochemical Society*, v. 141, n. 6, pp. 1421-1431, 1994.
- [16] JANG, D.H., SHIN, Y.J., OH, S.M., Dissolution of spinel oxides and capacity losses in 4 V Li / $\text{Li}_x\text{Mn}_2\text{O}_4$ cells, *Journal of The Electrochemical Society*, v. 143, n. 7, pp. 2204 - 2211, 1996.
- [17] LIU, H., WU, Y.P., RAHM, E., *et al.*, Cathode materials for lithium ion batteries prepared by sol-gel methods, *Journal of Solid State Electrochemistry*, v. 8, pp. 450-466, March 2004.
- [18] SUN, Y., YANG, Y., ZHAO, X., *et al.*, Synthesis and electrochemical characterization of $\text{LiNi}_{0.5}\text{Mn}_{1.5}\text{O}_4$ by one-step precipitation method with ammonium carbonate as precipitating agent, *Electrochimica Acta*, v. 56, n. 17, pp. 5934-5939, July 2011.
- [19] FANG, H.S., WANG, Z.X., LI, X. H., *et al.*, Exploration of high capacity $\text{LiNi}_{0.5}\text{Mn}_{1.5}\text{O}_4$ synthesized by solid-state reaction, *Journal of Power Sources*, v. 153, n. 1, pp. 174-176, January 2006.
- [20] ZHU, C., NOBUTA, A., SAITO, G., *et al.*, Solution combustion synthesis of LiMn_2O_4 fine powders for lithium ion batteries, *Advanced Powder Technology*, v. 25, n.1, pp. 342-347, January 2014
- [21] CHAVAN, S.V., TYAGI, A.K., Preparation and characterization of $\text{Sr}_{0.09}\text{Ce}_{0.91}\text{O}_{1.91}$, SrCeO_3 , and Sr_2CeO_4 by glycine–nitrate combustion: Crucial role of oxidant-to-fuel ratio, *Journal of Materials Research*, v. 19, n. 11, pp. 3181-3188, November 2004.
- [22] KINGSLEY, J.J., MANICKAM, N., PATIL, K.C., Combustion synthesis and properties of fine particle fluorescentaluminous oxides, *Bulletin of Materials Sciences*, v. 13, n. 3, pp. 179 – 189, June 1990.
- [23] SRIKESH, G., SAMSON NESARAJ, A., Synthesis and characterization of phase pure NiO nanoparticles via the combustion route using different organic fuels for electrochemical capacitor applications, *Journal of Electrochemical Science and Technology*, v. 6, n. 1, pp. 16-25, 2015.
- [24] YU, Z.M., ZHAO, L.C., Structure electrochemical properties of LiMn_2O_4 , *Transactions of Nonferrous Metals Society of China*, v. 17, n. 3, pp. 659 – 664, June 2007.
- [25] LEE, M.J., LEE, S., OH, P., *et al.*, High performance LiMn_2O_4 cathode materials grown with epitaxial layered nanostructure for Li-ion batteries, *Nano Letters*, v. 14, n.2, pp. 993-999, January 2014.
- [26] YANG, Z., WANG, Y., CHEN, X., *et al.*, Mg^{2+} and Ti^{4+} co-doped spinel LiMn_2O_4 as lithium-ion battery cathode, *Chemistry Select*, v. 4, n. 33, pp. 9583 - 9589, September 2019.
- [27] RAJU, K., NKOSI, F.P., VISWANATHAN, E., *et al.*, Microwave-enhanced electrochemical cycling performance of the $\text{LiNi}_{0.2}\text{Mn}_{1.8}\text{O}_4$ spinel cathode material at elevated temperature, *Physical Chemistry Chemical Physics*, v. 18, pp. 13074-13083, April 2016.
- [28] CAI, Z., MA, Y., HUANG, X., *et al.*, High electrochemical stability Al-doped spinel LiMn_2O_4 cathode material for Li-ion batteries. *Journal of Energy Storage*, v.27, pp. 101036, February 2020.
- [29] MIMANI, T., Fire synthesis – Preparation of alumina products, *Resonance*, pp. 50-57, February 2000.
- [30] KIMINAMI, R.H.G.A., Combustion synthesis of nanopowder ceramic powders, *Kona*, n. 19, pp. 156-165, 2001.
- [31] YU, Y., WANG, S., GUO, J., *et al.*, Facile synthesis of Ni-doped nano- LiMn_2O_4 ($0 \leq x \leq 0.10$) cathode materials and their electrochemical performances, *International Journal of Electrochemical Science*, v. 13, pp. 9950 – 9963, September 2018.
- [32] ARUNKUMAR, L., VIJAYANAND, H., BASAVARAJA, S., *et al.*, Combustion synthesis of LiMn_2O_4 by thermal decomposition of oxalate precursors, *Indian journal of Chemical Technology*, v. 15, pp. 41-44, January 2008.
- [33] NAGESWARA RAO, B., MURALIDHARAN, P., RAMESH KUMAR, P., *et al.*, Fast and facile synthesis of LiMn_2O_4 nanorods for Li ion battery by microwave assisted hydrothermal and solid state reaction methods, *International Journal of Electrochemical Science*, v. 9, pp. 1207-1220, 2014.
- [34] BASKARAN, R., SELVASEKARAPANDIAN, S., HIRANKUMAR, G., *et al.*, Dielectric and conductivity relaxations in PVAc based polymer electrolytes, *Ionics*, v. 10, n. 1-2, pp. 129 – 134, January 2004.
- [35] ARUN KUMAR, D., SELVASEKARAPANDIAN, S., NITHYA, H., *et al.*, Electrical properties of

cerium fluoride thin films, *Ionics*, v. 16, pp. 481-486, April 2010.

[36] PRABU, M., SELVASEKARAPANDIAN, S., REDDY, M.V., *et al.*, Impedance studies on the 5-V cathode material, LiCoPO₄, *Journal of Solid State Electrochemistry*, v. 16, n. 5, pp. 1833-1839, May 2012.

ORCID

Alagu Segar Deepi

<https://orcid.org/0000-0002-6136-7338>

Gopalakrishnan Srikesh

<https://orcid.org/0000-0002-1611-2133>

Arputharaj Samson Nesaraj

<https://orcid.org/0000-0003-0707-7804>